IIETA International Information and Engineering Technology Association
Advancing the World of Information and Engineering

Journal Européen des Systèmes Automatisés
Vol. 56, No. 4, August, 2023, pp. 627-639
Journal homepage: http://iieta.org/journals/jesa

A Low-Cost, Modular, Cable-Driven, Anthropomorphic Robotic Hand: A Conceptual Design and Application in Biomimetic Study

Daniel O. Adejumo[1], David A. Fadare[1], Rasaq A. Kazeem[1,2], Omolayo M. Ikumapayi[3,4*], Ayodeji Falana[1], Adebayo S. Adedayo[1], Dorcas A. Fadare[5], Adeyinka O. M. Adeoye[3], Adebayo T. Ogundipe[6], Elisabeta S. Olarinde[7]

[1] Department of Mechanical Engineering, Automation and Robotic Laboratory, University of Ibadan, Ibadan 200281, Nigeria
[2] Department of Mechanical Engineering Science, University of Johannesburg, Auckland Park Campus, Johannesburg 2092, South Africa
[3] Department of Mechanical and Mechatronics Engineering, Afe Babalola University, Ado Ekiti 360101, Nigeria
[4] Department of Mechanical and Industrial Engineering Technology, University of Johannesburg, DFC, Johannesburg 2092, South Africa
[5] Department of Chemical Sciences, Anchor University, Lagos 112106, Nigeria
[6] Directorate of Information Communication Technology, Afe Babalola University, Ado Ekiti 360101, Nigeria
[7] College of Law, Afe Babalola University, Ado Ekiti 360101, Nigeria

Corresponding Author Email: ikumapayi.omolayo@abuad.edu.ng

https://doi.org/10.18280/jesa.560412

Received: 1 June 2023
Revised: 10 August 2023
Accepted: 21 August 2023
Available online: 31 August 2023

Keywords:
biomimetic, anthropomorphic, robotic hand, automation, reinforcement learning

ABSTRACT

The UI Hand I robot is the pioneering development of an anthropomorphic robotic hand for pushing the limits of dynamic biomimetic anthropomorphic robotic hand study in Nigeria. The objective of this research is to develop a truly anthropomorphic hand that captures all the DOF of the hand and can reproduce the dexterity of the human hand. Many robotic hands have been developed so far, but many still lack true anthropomorphism; many have used mechanisms different from those adopted by the human hand, leading to significant deviations both in form and function. Our work aims to improve the fidelity of biomimetic robotic hand design. To this end, we present the conceptual design of a biomimetic, low-cost, modular, cable-driven, tele-operated 26 degrees of freedom anthropomorphic robotic hand. We understudied the biomechanics of important features of the anatomy of the human hand and wrist, developed appropriate mechanical models that mimic the mechanics of these features, and compared them with the CT scan of an actual human hand. The robotic hand's links were designed in Fusion 360 and 3D printed in PLA. The muscles and tendons were modelled as a pulley-cable system using 0.46 mm Spectra® fiber for the tendons, and micro electric motors were used for actuation. A Raspberry Pi 4 was used as the controller, the leap motion controller as the teleoperation device, and Deep Reinforcement Learning was used to learn a suitable control policy. The proposed (UI hand I) anthropomorphic robotic hand and wrist model comprises 29 bones and 17 composite joints with 26 degrees-of-freedom. A total of 80 components were used to model the bones and joints with an estimated weight of 450g. With the addition of the motors, battery and other electrical components, the upper limit of the estimate is 1.2 Kg. The estimated cost of the project is $ 1, 241.80. The research aims to evaluate the robotic hand's dexterity in teleoperation and achieve the full range of poses in the human hand, with potential implications including enhanced automation in spacewalks, construction, industrial operations, and prosthetics.

1. INTRODUCTION

It is generally accepted that the cost of time and grant funding on developing a research-oriented, custom-designed anthropomorphic robotic hand is often prohibitive [1]. The manipulation of a robotic hand is dependent on many design parameters, such as the finger length, the range of motion (ROM) of the joints, the weight of the robotic hand, or transmission types [1]. Traditional end-effectors in robotic arms such as 2-fingered grippers are good at what they do, but they are specialized for a single or few tasks. Having an end effector, a robotic hand that is not just a tool, but can manipulate a wide range of tools and objects is of immense impact. Such a robotic hand is also of immense use in prosthetics for hand rehabilitation. But as we have built things around us for humans and the real world is so uncertain, such a robotic hand must possess the dexterity and robustness close to its human counterparts. Human hand dexterity is quite personal, with significant variations in bone lengths and shapes, muscle insertions, and even the presence or absence of certain muscles [2]. To push the limits of dynamic biomimetic anthropomorphic robotic hand study, it is important for researchers to have fast and easy access to modify any design parameters and conduct fearless experimentation. Our goal is to build a robotic hand that is close to the human hand in terms of the degree of freedom, range of motion, compliance, and

object manipulation strategies [3]. The Automation and Robotic laboratory of the Faculty of Technology, University of Ibadan is set to provide a platform for pushing the limits of dynamic biomimetic anthropomorphic robotic hand study in Nigeria. The UI hand I is our pioneering effort with great potential that can be scaled up, modified, and trained to accomplish complex tasks. In the nearest future, we look forward to having anthropomorphic robotic hands trained to play the keyboard and beat our local drums like “Bata” and “Gangan”.

In the literature, several robotic hands with different degree of anthropomorphism and dexterity have been developed with varying mechanical design, adopted sensory system and control architecture. Xu et al. [1] described the design process for a 20-degree-of-freedom, cable-driven, anthropomorphic robotic hand. In order to effectively evaluate the kinematic arrangement, the survey used a custom-designed physics engine to simulate the robotic hand. Studies showed that force behaviours, tactile sensing, and actuation speed are all very good. In simulated studies, Rajeswaran et al. [4] demonstrated that model-free deep reinforcement learning techniques can efficiently upgrade to extremely complicated robotic manipulators with a high-dimensional 24-DOF hand and fix them from inception to completion. Moreover, Liow et al. [5] suggested an entirely modular system for a mechanical arm with wrist and finger level configurability, enabling the attachment and removal of tendon driven fingers without instruments, rewiring or retendoning. The experiments have demonstrated that the prosthetic hand can capture a diverse range of domestic and food products of varying size, shape and weight without ejecting fingers and gives the user the ability to discard them effortlessly with a single hand. Mnyusiwalla et al. [6] demonstrated a new robotic hand capable of fine inside-hand adaptive and manipulation grasping. The robotic hand is outfitted with fingers based on a human anatomical finger model. Tendon-based actuation uses tendons to minimise kinematic, friction, and static coupling between different finger axes. The findings demonstrated that the finger motion has outstanding dynamic characteristics and precision. Ultimately, the novel finger design resulted in the creation of a fully actuated prosthetic hand with four fingers and 16 degrees of freedom. Additionally, a cheap, 3D printable, small, and light robotic hand was created by Tian et al. [7]. The robotic hand has 6 Degrees of Freedom and a mass of 150 g, and it has 15 joints that are comparable to those in a genuine human hand. Six tiny actuators were all that were needed to move the robot arm. Dependably incorporated into the hand model is the wrist connecting component, which can be altered to fit different robots.

A five-fingered anthropomorphic gripper was designed in their study (Mańkowski et al. [8]) for manipulating stretchy components. The manipulator had a hybrid design with two tendon-driven digits for reliable power grasping and three fully operated fingers for precise manipulation. The design makes use of as many commercially available and 3D-printed components as is practical for ease of replication. An innovative tendon-driven, bio-inspired prosthetic hand structure for in-hand manipulation was proffered by Vulliez et al. [9]. The progression of tendon routing from the Laboratoire de Mécanique des Solides hand to the new RoBioSS dexterous hand was the central subject of their research. Between actuators and joints, the new design's motion transmitter generates only linear coupling connections. Results from experiments utilizing an identical procedure for the old hand and the new hand show how the mechanical design has improved over time. The mechanical performance of robotic fingers could be improved, greatly simplifying the hand control software. Furthermore, Wang et al. [10] unveiled a novel configurable tactile sensory dexterous hand for household robotic systems. The fully actuated hand has one palm and three fingers, as well as integrated tactile detectors, control boards and motors. The palm and each finger have two degrees of freedom. The modular architecture makes it simple for even non - technical users to detach and attach the hand. The tactile sensor module with a new arrangement can help to reduce detector number while maintaining sensitivity. A number of tests were carried out to test the detector unit and assess hand effectiveness with an object set. The results demonstrated that the sensor module could provide accurate sensing results as well as recognise constant vibration data, and that the hand has exceptional grasp potential. Additionally, Li et al. [11] demonstrated a general-purpose prosthetic hand with customizable antagonistic fingers and adhesive soft modulations capable of grasping and manipulating. The modular antagonistic fingers, hand-like configuration, compliant joints, soft modulations, and tendon-driven actuation inspired by the human hand with rigid and soft structures are all part of the anthropomorphic design. The robotic hand is made up of five fingers that have numerous joints and a palm that has two joints. Through conceptual coupling, the components can be quickly assembled to modify the degrees of freedom and finger length for variable-workspace manipulation/grasping. The study findings confirmed the soft adhesive modulations and the robotic hand's ability to perform different types of manipulation/grasping.

He et al. [12] designed the prosthetic hand in accordance with the anatomic structures of the hand and took these structural characteristics into consideration when creating the robotic hand in a bid to develop one that is as flexible as a prosthetic hand. A grabbing demonstration was carried out using simple objects from daily life to assess how well the planned prosthetic hand would perform in real-world situations. The outcomes demonstrated the high performance and realistic appearance of the suggested prosthetic hand. On top of that, a low-cost 3-axis fingertip force sensor for robotic manipulation was described by Xu et al. [13]. The design makes use of 3D printing technology to its fullest potential and takes crucial aspects like modification and maintainability into account. The end product is a sensor with a removable fingertip made of 3D-printed materials and a cantilever mechanism that enables the detection of contact forces using three readily available, reasonably priced force sensors. Tian et al. [14] outlined a quick and efficient process that combines digitization and 3D printing methods to turn a physical hand into a cable-driven robotic hand that is printable in three dimensions. The procedure entails sectioning the 3D digitised hand model, including joints, and turning it into a 3D printable model. Their solution, which was obtained through 3D scanning, maintains over 90% of the geometrical information of a human hand1 when compared to other robotic strategies. A comprehensive review on anthropomorphic robotic hands development can be found in Gama Melo et al. [15]. Although significant amount of work has been carried out in this area, but most anthropomorphic hands are still expensive, driven by expensive pneumatic actuators, or do not have many of the degrees of freedom found in the human hand. Significant work was done by Xu et al. [1] to create a low-cost, modular, 20-

DOF robotic hand. This is also powered by pneumatic actuators, increasing the cost of the system, and the biomechanics can still be greatly improved. Further work on this (Xu and Todorov [16]) resulted in a significantly improved hand, but without the wrist incorporated yet. We present a 26-DOF system, actuated by motors to reduce cost, and incorporates a wrist. With a wrist incorporated, our robotic hand can easily be attached to an existing robotic arm, increasing its versatility. Our approach is to first understand the important mechanical features of the hand, and then develop mechanical models of these features and compare with the human hand. This will result in a mechanical hand that mimics the human hand with a higher degree of freedom and range of motion.

1.1 Anatomy of the human hand

Anatomically, the major mechanical structures of the human hand are bones; bone articulations (joints); muscles and tendons; and ligaments [17, 18]. There are a total of 29 bones, 5 types of bone articulations, and more than 30 muscles in the human hand and wrist [19]. These work together to create the flexion, extension, adduction, abduction, and axial rotation movements (Figure 1) observed in the human hand and wrist.

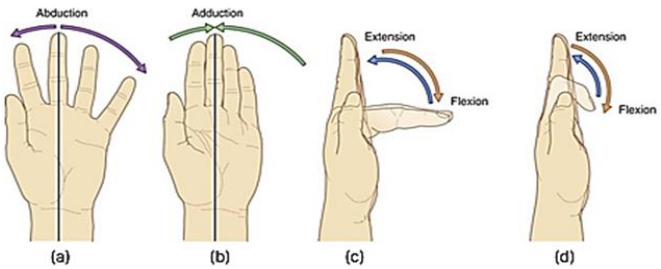

Figure 1. Movements at the joints of the hand: (a) Abduction; (b) Adduction; (c) Flexion/Extension at the MCP joint; (d) Flexion/Extension at the IP joint (Basic Medical Key, 2022)

In naming and describing the various parts of the hand, various anatomical terms are commonly used. These terms are defined next. Anterior, Posterior, Palmar, Dorsal, Lateral, Medial, Radial, Ulnar, Proximal, and Distal are used to describe an area on a part or the direction in which a part is relatively positioned in the hand. Anterior or palmar describes a direction towards the palm of the hand, while posterior or dorsal describes a direction towards the back of the hand. Lateral or Radial(is) describes a direction towards the thumb of the hand in question, while medial or ulnar(is) describes a direction towards the little finger of the hand in question. Distal describes a direction upwards, while proximal describes a direction downwards towards the thumb. The terms adduction, abduction, flexion, and extension are used to describe the different movements of the joints of the hand. The term adduction describes rotation towards the centreline of the hand, while abduction describes rotation away from the centreline of the hand. The centreline passes through the middle finger down to the wrist. Flexion describes rotation towards the palmar surface of the hand, while extension describes rotation away from the palmar surface of the hand. The term 'Digitorum' in part names refers to the digits of the hand; the term 'Digiti Minimi' refers specifically to the little finger; and the term 'Pollicis' refers specifically to the thumb.

1.1.1 Bones

The bones of the hand are grouped into carpals, metacarpals, and phalanges [20]. The other two bones that make up the wrist are the radius and ulna in the forearm (Figure 2a). Fingers II to V have 3 phalanges each (distal, middle, and proximal phalanges), while digit I has only 2 phalanges (distal and proximal phalanges). The metacarpals are the long bones occupying the bulk of the palm area [21]. Each finger has a metacarpal bone just below (*proximal to*) the proximal phalanx. The long bones - phalanges and metacarpals - have a head and a base where they articulate with neighbouring bones (Figure 2b). The geometry of the articulation surface contributes to the degree of freedom and range of motion at these articulations.

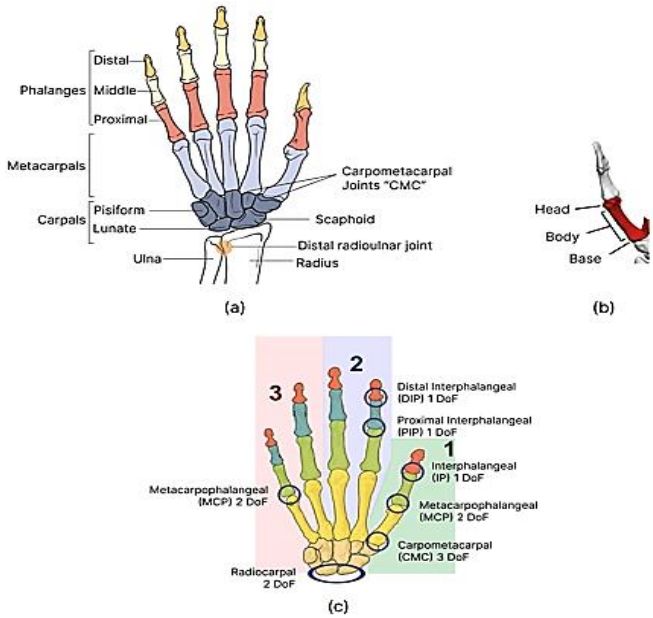

Figure 2. (a) Bones of the hand and wrist; (b) Head, body (shaft) and base of long bones; (c) Joints of the hand and wrist [22]

1.1.2 Bone articulations (joints)

There are five important types of bone articulation found in the hand and wrist - the radiocarpal, intercarpal, carpometacarpal, metacarpophalangeal, and interphalangeal joints (Figure 2c) [22]. The radiocarpal joint is formed between the radius and carpal bones and allows for flexion/extension and adduction/abduction at the wrist (2 DOF). The intercarpal joints are formed between the carpal bones. The intercarpal joints are relatively fixed as only slight movements are observed there. The carpometacarpal (CMC) joints are formed between the carpals and metacarpal bones and are fixed joints for digits II to IV. The CMC joint for digit I (CMC I, also called TMC) allows for flexion/extension, adduction/abduction, and axial rotation movements (3 DOF) at the base of the thumb. CMC V also allows for movements like CMC I but very slightly. To allow for the degree of freedom at the CMC joint, the articulation surface geometries at the CMC I joint are roughly complementary saddle surfaces. The metacarpophalangeal (MCP) joints are formed between the metacarpals and the proximal phalanges [23]. The MCP joints allow for flexion/extension and adduction/abduction movements (2 DOF) of the proximal phalanges. For MCP II - V, the articulation surface geometries are roughly spherical. The interphalangeal (IP) joints are formed between the

phalanges of the digits, allowing for flexion/extension movements (1 DOF) of the middle and distal phalanges. Digits II to V have two interphalangeal joints each: the distal interphalangeal (DIP) and proximal interphalangeal (PIP) joints. Digit I have only 1 IP joint between its distal and proximal phalanges. The articulation surface geometries at the IP joints are roughly cylindrical.

1.1.3 Muscles and tendons

The muscles of the hand are divided into intrinsic muscles (Figure 3) and extrinsic muscles (Figure 4). The intrinsic muscles have their origin within the hand and attach to the bones within the hand. The intrinsic muscles include the Dorsal Interossei, the Palmar Interossei, the Lumbricals, the Thenar muscles, and the Hypothenar muscles. The extrinsic muscles have their origin outside the hand, within the forearm, and attach to the bones within the hand. The extrinsic muscles include the Flexor Digitorum, the Extensor Digitorum, some Pollicis, and Carpi muscles [24].

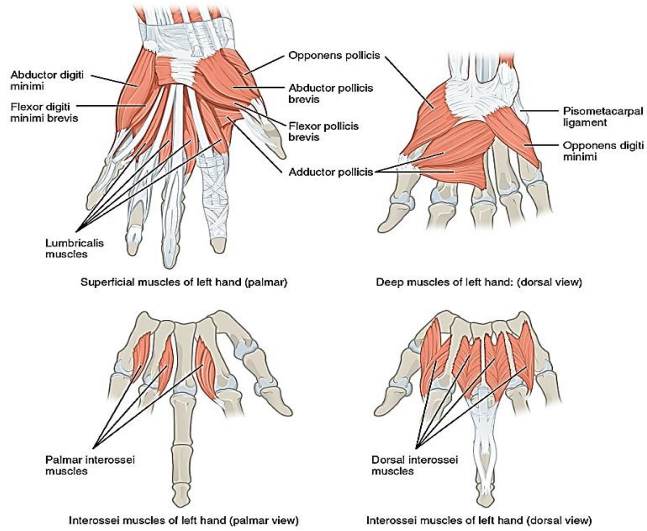

Figure 3. Intrinsic muscles of the hand [24]

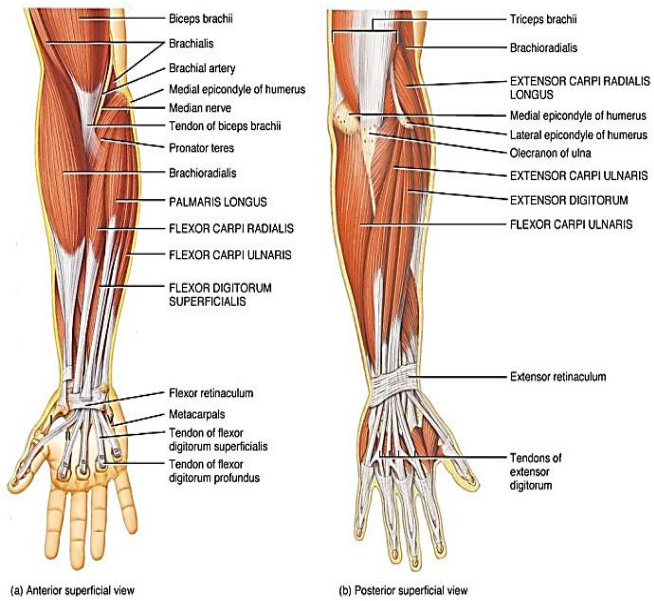

Figure 4. Extrinsic muscles of the hand [24]

The Dorsal Interossei are four in number, and they are each responsible for abduction of the digits 2 to 4 at the MCP joint. The Palmar Interossei muscles are each responsible for the adduction of the digits 2, 4, and 5 at the MCP joint. (Digit 3 has no palmar interosseous muscle but has two dorsal interossei). The Dorsal and Palmar Interossei also serve the function of flexion at the MCP joints and extension at the IP joints via the extensor hood mechanism of the digit they each attach to. The lumbrical muscles are four in number, and each produces flexion at the MCP joints of digits 2 to 5 and extension at the IP joints via the extensor hood mechanism of the digit they attach to. The Thenar muscles are four muscles that act on the thumb. These include the adductor pollicis, which primarily functions to adduct the thumb at its CMC joint; the abductor pollicis brevis, which abducts the thumb at its CMC joint; the flexor pollicis brevis, which flexes the thumb at its MCP and CMC joints; and the opponens pollicis, which primarily functions to produce thumb opposition at the CMC joint. The Hypothenar muscles include the abductor digiti minimi, which primarily abducts and flexes digit 5 at its MCP joint; the flexor digiti minimi, which flexes digit 5 at its MCP joint; the opponens digiti minimi, which functions to flex and laterally rotate digit 5 at its CMC joint; and the palmaris brevis, which helps to wrinkle the skin over the hypothenar eminence [24].

The Flexor Digitorum Superficialis muscles each insert on the middle phalanx of digits 2 to 5 and produce flexion at the PIP and MCP joints. The Flexor Digitorum Profundus muscles each insert on the distal phalanx of digits 2 to 5 and produce flexion at the DIP, PIP, and MCP joints. The Extensor Digitorum muscles each insert into the extensor hood of digits 2 to 5 and produce extension at the IP and MCP joints. The Extensor Pollicis Brevis inserts on the dorsal surface of the base of the proximal phalanx of the thumb and produces extension at its MCP and CMC joints. The Extensor Pollicis Longus inserts on the dorsal surface of the base of the distal phalanx of the thumb and acts to produce extension at its IP and MCP joints. The Flexor Pollicis Longus inserts on the palmar surface of the distal phalanx of the thumb and flexes the thumb at its IP and MCP joints. The Abductor Pollicis Longus abducts and extends the thumb at its CMC joint. The Flexor Carpi Radialis flexes and abducts the wrist; the Flexor Carpi Ulnaris flexes and adducts the wrist; the Extensor Carpi Radialis extends and abducts the wrist; and the Extensor Carpi Ulnaris extends and adducts the wrist [24].

The muscles terminate in tendons, which insert into the bones that they actuate. The actions of the muscles are contraction and relaxation only. Different muscles also work together to achieve fine control of the joints through the co-contraction of the muscles [25].

1.1.4 Ligaments

Ligaments provide structures that hold the bones in place at the joints and limit the range of motion as depicted in Figure 5. They also provide structures that serve as tendon tunnels to hold the tendons in place and close to the bones during movement. Hence, the ligaments of the hand perform the functions of stabilising joints, limiting the range of motion, and providing a routing tunnel for the alignment of the tendons. The ligaments of the hand are associated with different joints and bones of the hand. Associated with the phalangeal bones are the annular and cruciform ligaments on the palmar aspect of the phalanges. These ligaments provide small tunnels through which the Flexor Digitorum tendons pass. They

facilitate the smooth gliding of the Flexor Digitorum tendons, keep them attached to the phalanges during movement, and allow for force distribution from the tendons to the phalanges. Associated with the interphalangeal joints are the palmar interphalangeal ligaments and the collateral interphalangeal ligaments. The palmar interphalangeal ligaments prevent hyperextension, while the collateral interphalangeal ligaments prevent excessive adduction-abduction movement at the interphalangeal joints. At the metacarpophalangeal joints, the palmar metacarpophalangeal ligaments prevent hyperextension. At the carpometacarpal joints, the dorsal carpometacarpal ligaments and palmar carpometacarpal ligaments stabilise the carpometacarpal joints and limit gliding movements. The flexor retinaculum ligament of the wrist stabilises the carpal bones and provides a tunnel for the flexor tendons. Similarly, the extensor retinaculum ligament of the wrist stabilises the carpal bones and provides a tunnel for the extensor tendons of the hand.

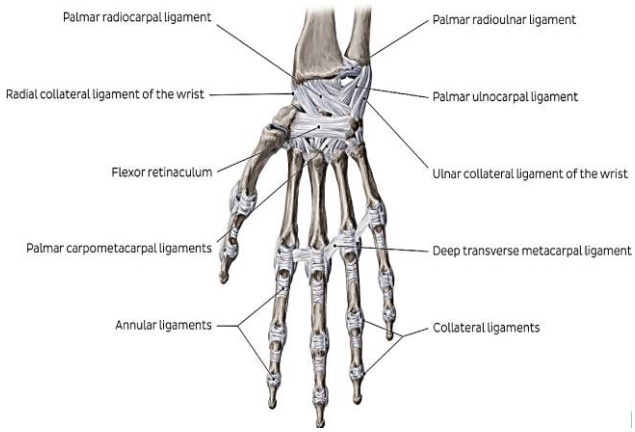

Figure 5. Ligaments of the hand and wrist [24]

2. METHODOLOGY

2.1 Modelling of bones and joints

Appropriate mechanical models that mimic the mechanics of the hand and wrist were modelled using Fusion 360 software, with all kinematic data of the bone and joints taken from the CT scan's mesh (Figure 6) of an actual human right hand developed by the Visible Human Project [26]. Each phalanx of the digits is modelled as a single link, providing insertion point structures for the tendons and the extensor hood attached to it. The carpal bones and metacarpals II-IV have no *significant* relative motion between them, and so they are modelled as a single link, the carpals-metacarpals link. Metacarpals I and V are modelled as separate links since they can move at their CMC joints. The tendons are motor driven, so the carpals-metacarpals link, metacarpal I, and V links also provide structures for the attachment of the intrinsic motors (muscles). The base of the carpals-metacarpals link also provides insertion point structures for the tendons attached to the carpals.

While the interphalangeal joints have more intricate motion and the rotation axis is not fixed, they can be effectively approximated as revolute joints. To allow for a modular design and fast prototyping, snap-on joints are employed at all joints in the hand [1]. Also, instead of ligaments, hard stops are used to provide joint limits at all joints in the hand. While this reduces compliance, we focused on the DOF and ROM for this design, and compliance will be addressed in the next iteration.

Like the IP joints, the MCP joints have a more intricate motion, but the major movements are modelled with a universal joint, except for MCP I, which we model as a revolute joint. We modelled the CMC joint with three revolute joints. Two revolute joints with perpendicular rotation planes and a vertical offset between their axes of rotation were used to model flexion/extension and adduction/abduction. With this arrangement, the locus of a point on the follower link draws out a saddle surface, like the articulation surface geometry observed at the CMC I joint. The axis of the third revolute joint is perpendicular to the first two and located vertically between these axes. The third revolute joint allows for axial rotation at the CMC joint. We modelled the RC joint with two perpendicular revolute joints. While in the human hand, the rotation axis for adduction/abduction is mostly distal to the axis for flexion/extension during movement, this arrangement will affect the grasping in our robotic hand which uses revolute joints, or it will push the RC joint too low into the forearm. Instead, we have positioned the axis for flexion/extension distal to the axis for adduction/abduction. We hope the control system will learn to adapt to this uniqueness and still achieve dexterity.

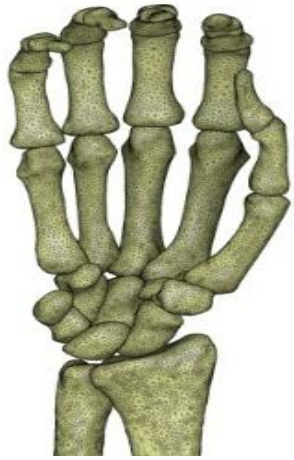

Figure 6. CT scan image of the right hand and wrist [26]

2.2 Modelling of muscles and tendons

A tendon-based transmission system is used to model the action of the muscles and tendons in the hand. Tendon-based transmissions have been widely used in actuating dexterous robotic hands [27]. Tendon transmission makes it possible to place the actuators of joints remotely from the joints they actuate, allowing for more actuators to be included for control of more degree-of-freedoms in the hand. This design also reduces the inertia and mechanical complexity of the actuation system, allowing for improved morphology of the hand. Nazma and Mohd [27] presented a review on tendon driven robotic hands. Hence, a muscle and tendon are modelled as a pulley-cable system. A tendon-cable is attached to a pulley which is actuated by a motor. (The selection procedure for the motors is further discussed in section 2.4). Contraction is mimicked by driving the pulley in a direction that reduces the cable length, and relaxation by applying zero torque on the pulley. The tendon-like cables transmit force to the bones to actuate the different joints. Certain muscles of the hand have more than one insertion point, e.g., the *Extensor Digitorum*

Communis. The *Extensor Hood* structure attached dorsally to the phalanges facilitates this behaviour [28]. Effectively, this can be seen as different fibres of the same tendon travelling to insert at different points. We model this by having different cables from the same pulley inserted at the different insertion points of the muscle, and the different cables of the same pulley are made to pass through the same route.

Sliding surfaces positioned along the bone links are used to route the tendons. While the use of sheaths is a convenient solution, it introduces distributed friction along the tendon, which introduces hysteresis and dead zones in the transmission system characteristics [29-31]. To reduce friction and wear of the sliding surfaces, the tendon surface must be smooth. We adapted 0.46 mm Spectra® fiber for our tendons [1]. Spectra fiber demonstrates high strength, stiffness, smoothness, abrasion resistance, and virtually no spool memory. This is very well suited for our application.

2.3 Measuring similarity of CAD model and CT scan

Our model has a *visually appealing* appearance but, we'll like to evaluate how similar it is to the reference CT scan and the human hand in general. For this we computed an Intersecting Volume Ratio (IVR) which we define as shown in Eq. (1):

$$IVR = \frac{Intersecting\ vol.\ of\ \text{model}\ and\ CT\ scan}{Vol.\ of\ \ mod\ el} \tag{1}$$

This ratio tells us how much of the 3D volume of our model is common to the model and the CT scan, and it serves as a numerical evaluation of similarity between our model and the CT scan. To compute the IVR, the first step is to match the orientation of the two 3D models. The orientation is adjusted iteratively until a maximum intersection volume is obtained. We did this step manually, but it can also be algorithmically determined. Next, the intersecting volume and the volume of the CAD model are evaluated, and the IVR is computed according to Eq. (1).

2.4 Determination of actuators specifications

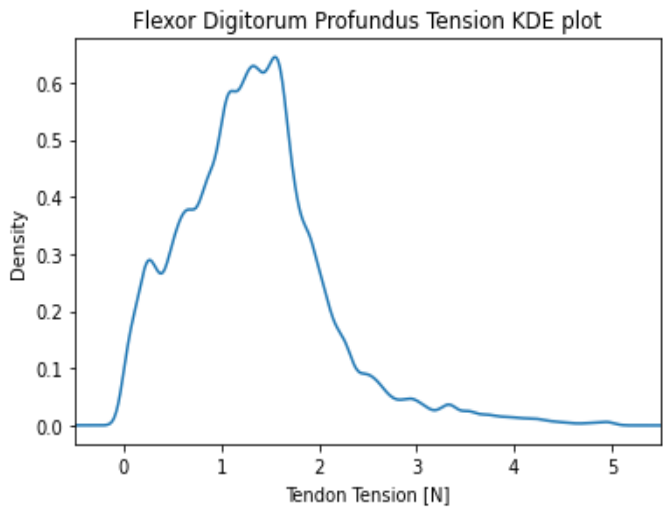

Figure 7. Tension distribution for the flexor digitorum profundus tendon

Torque controlled DC motors will be used to drive the tendons. To specify the motors for the hand we first trained a reinforcement learning (RL) agent for direct tendon force control [32]. The same agent will control the physical robot hand. (Details of the RL control is provided in sections 2.7 and 3.4). We perform rollouts on thousands of teleoperation targets and collect data of the tensions applied to each of the tendons by the agent to reach the targets. This gives us a distribution of the tension required for each tendon during operation. This tension distribution is then used in providing a specification for the motor of each tendon. A sample tension distribution from preliminary results is shown in Figure 7.

The motor torque is obtained with Eq. (2).

$$Motor\ Torque = Tendon\ tension \times Pulley\ radius \tag{2}$$

To specify a tendon's motor torque capacity, a representative value for tendon tension from the tension distribution is used in the motor torque equation. The value depends on the nature of the distribution. Usually, a value between the 75th percentile and the max will be chosen. This torque capacity is validated by fine-tuning the agent on the new tendon tension limit and verifying that control is achieved. The initial tendon tension upper limits are from high guesses, the agent optimizes for tension magnitude and uses the lowest possible tendon tension for control. Suitable values for the pulley radii are determined as the design progresses. The instantaneous motor power is obtained with Eq. (3).

$$Motor\ power \approx Tendon\ power = Tendon\ tension \times Tendon\ linear\ speed \tag{3}$$

A distribution of the tendon power is also obtained from the rollouts by the agent. To specify the motor power capacity, a representative value from the distribution is also chosen depending on the nature of the distribution.

2.5 Computing and communication system

A Raspberry Pi (RPi) 4 Model B is chosen as the main computer of the system. With a 4GB RAM and a Quad Core processor @ 1.5GHz, this board will run the RL model, handle communication, and other software demands for the teleoperation of the hand. The RPi is also responsible for controlling the 34 motors in the hand via appropriate Hardware Attached on Top (HAT) modules. The HATs make it possible to control multiple PWM outputs via just two 12C pins. RPi communicates with the HAT via 2 12C pins, while the HAT handles PWM without any processing overhead on RPi. (A single Adafruit PWM HAT can control up to 16 PWM outputs, and features stacking up to 62 HATs to get even more PWM outputs). RPi will run the control loop at a sampling frequency of 12.5 Hz to control the motors. This follows from the action time (time between torque commands) of the RL agent as discussed in section 2.7. As part of the domain randomization in training the RL agent is randomizations on the action time, so that agent is robust to possible variations in the action time. While the RPi has a fast enough processor, this consequently relieves the strict timing requirement on the control loop.

2.6 Deep Reinforcement Learning (RL) control

The control approach is to move the fingertips of the robotic hand to the fingertips poses of the operator (teleoperation). In

the human hand, contraction of a muscle to flex or extend a joint tends to flex or extend the joints proximal to (below) that joint too [33]. For instance, contraction of the *Flexor Digitorum Superficialis* to flex the PIP joint also results in flexion at the MCP and wrist joints [34, 35]. This behaviour translates to the anthropomorphic robotic hand too. Hence, control of the hand requires a robust control system that can handle the complexities and uncertainties of the anthropomorphic robotic hand. For robust control, we used Deep RL to train a model that can learn a suitable policy to control the hand. Our RL model was implemented and trained using the Stable Baselines3 (SB3) library. Stable Baselines3 (SB3) is a set of reliable implementations of reinforcement learning algorithms in Python, built on top of the PyTorch library. The Soft Actor-Critic (SAC) algorithm from SB3 was used in training our RL agent. SAC is an off-policy, max-entropy algorithm, and its design aligns well with the challenges posed by robotic tasks, making it a popular choice for improving the performance and adaptability of robotic control systems [36, 37]. Yu and Wang [38] present a review on dexterous manipulation for multi-fingered robotic hands with reinforcement learning.

Our RL agent was trained in a Mujoco Simulation of the hand. The observation is the cartesian positions of the fingertips, the targets, and the velocity of the fingertips. The action space is continuous, the action is the tension applied to each tendon, and the time between actions (action time) of the agent is 80 ms [39]. The target for each episode is randomly sampled from the workspace of the fingertips, and the environment is solved when all fingertips come within a distance threshold to the target. The reward function is adapted from the work of Caggiano et al. [40] and is given by Eq. (4).

$$\begin{aligned} &-\left(w_1 \times \text{reach\_dist}\right) + w_2 \times ((\text{reach\_dist} < 2 \times \text{solve\_th}) \\ &+(\text{reach\_dist} < \text{solve\_th})) - \left(w_3 \times \text{act\_mag}\right) \\ &-w_4 \times (\text{reach\_dist} > \text{far\_th}) \end{aligned} \tag{4}$$

Where *reach_dist* is the distance of the fingertips to the target, *solve_th* is the distance threshold of the fingertips to the target below which the environment is solved, *act_mg* is the magnitude of the tension applied to the tendons; *far_th* is the distance threshold above which the fingertips have moved too far from the target and the episode is terminated. w_1, w_2, w_3 and w_4 are weighting factors for each term in the reward function.

The performance of the control approach is evaluated on the satisfactory achievement of different poses in the human hand when the robotic hand is teleoperated on a variety of human tasks. The hand is teleoperated for an extended period of time on various human tasks - operating machines and handling tools, operating a computer, driving a vehicle, etc. The operator's hand poses are sampled during the operation and replicated on the robotic hand at up to 12.5 Hz. The evaluation metrics used are the average position error and the time delay error in replicating the operator's hand poses for different tasks. An optimal performance minimises these metrics below set thresholds.

Solving the control problem in simulation doesn't guarantee performance in the real world [38]. Several factors such as friction, material properties, and sensor inaccuracies, can lead to discrepancies that affect the hand's performance when deployed in real-world scenarios. Several Simulation to Real (Sim2Real) robot transfer techniques are used to address this problem. We'll apply Adaptive Domain Randomization from the work by Akkaya et al. [41] to ensure that the policies learned by the agent in the Mujoco Physics simulator transfer to the real world. To further tackle the potential challenges of discrepancies that might arise between simulation and the real world, we'll use techniques such as domain adaptation, fine-tuning with real-world data, and reinforcement learning from human feedback to assist in handling uncertainties and improving the adaptability of the system.

The trained agent is further used down the design pipeline to determine the specifications for the motors that will drive the tendons. The distribution of the tension used by the agent during control are collected from simulation and used to determine the required motor torque and power capacity as described in section 2.4. Section 3.4 presents preliminary results on the use of SAC for controlling a single finger and data from simulation for determining motor specifications.

2.7 Teleoperation

For teleoperation of the hand, a hand motion capture device to track the pose of an operator's fingertips is required. We have chosen the Leap Motion Controller (Figure 8), which is effective for our application and cheap compared to most motion capture gloves. The device plugs in via USB to a host computer, from where pose target commands can be sent wirelessly to the robotic hand.

Figure 8. Leap Motion Controller [42]

3. RESULTS AND DISCUSSION

3.1 The 3D model of bones and joints

Based on the mechanics model of the bones and joints, CAD models of the bones and joints were created in Fusion 360. This results in a model that geometrically resembles the human hand (Figure 9). The detailed model of the Phalanges and IP joints, CMC joint and the RC joint are shown in Figure 10. The overall dimensions of the hand are 250 × 105 × 45 mm (Figure 11) which falls in the range of the dimensions of the human hand. The 3D model will be 3D printed using Polylactic Acid (PLA) filaments. With PLA the total mass of the system is ~450 g, which also falls in the range of the mass of a normal human hand.

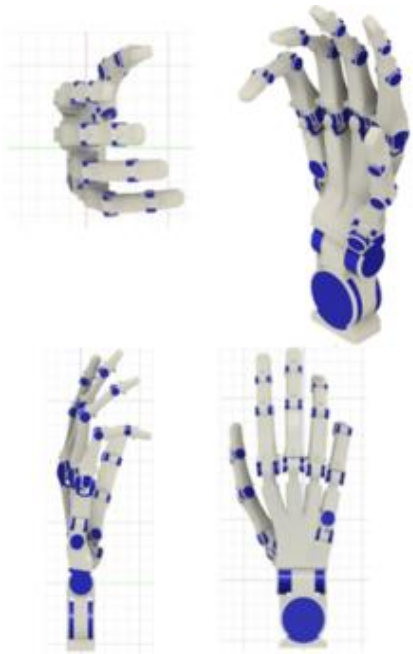

Figure 9. 3D model of the UI Hand I

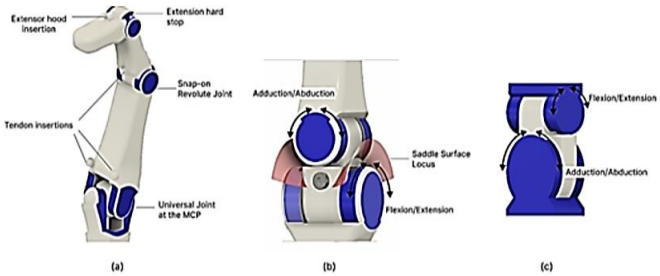

Figure 10. Detail of the mechanics model of the bones and joints: (a) Phalanges and IP joints; (b) CMC joint; (c) RC joint

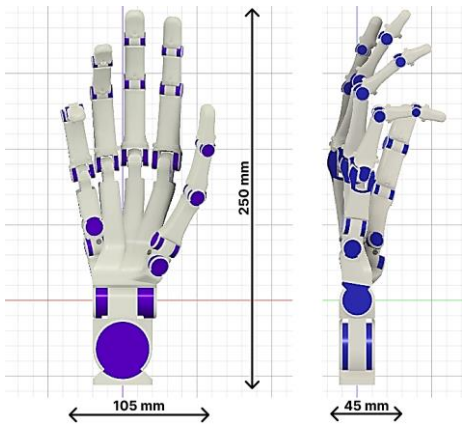

Figure 11. Overall dimensions of the hand and wrist

3.2 Comparison of the developed model with the CT scan's mesh

Figure 12 shows our model of UI Hand I overlaid with the CT scan of the hand and wrist for comparison. The CT scan of the hand is that of a normal human (female, adult) from the visible human project [43]. Because all kinematic data were read off the CT scan's mesh, all links in the model can be seen to share the same kinematic length and pose with the corresponding link in the CT scan.

We computed the Intersecting Volume Ratio (IVR) according to Eq. (1). After matching the orientation of the CAD model and the CT scan's mesh, the IVR is computed accordingly. Table 1 shows the results of the IVR computation for the wrist, carpals, and metacarpals region of the hand. The IVR is smaller when computed with the mesh of the bones only. We can obtain a higher IVR by computing with the CT scan of the full hand which includes the flesh covering, and this approach will be employed in further work.

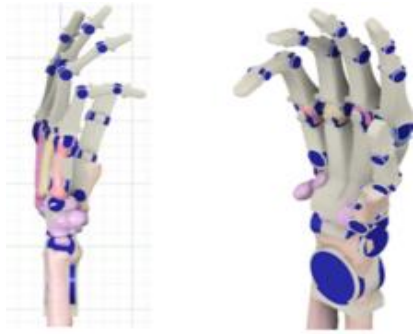

Figure 12. Comparison of the proposed model with CT scan of the human hand and wrist

Table 1. IVR for the wrist, carpals, and metacarpals region

Parameter	Value
Intersecting volume	7.254E4 mm^3
Model's volume	1.218E5 mm^3
IVR	0.60

3.3 Model of muscles and tendons

The pulley-cable actuation system model of the muscles and tendons was created in the Simscape Multibody software. Figure 13 shows the pulley-cable actuation system of the index finger, including its *Palmar Interossei*, *Dorsal Interossei*, and *Extensor Digitorum Communis* muscles. To model the *Extensor Hood Mechanism*, 3 cables originate from the pulley of each of these muscles. These cables then insert at the corresponding insertion points of the muscle and the Extensor Hood, one cable per insertion point.

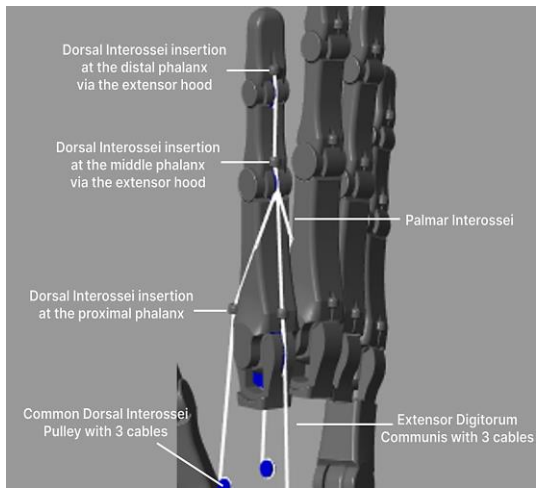

Figure 13. 3D model of the pulley-cable actuation mechanism showing the origin and insertion points of the muscles

3.4 Preliminary results on reinforcement learning control

As part of the preliminary efforts, we successfully used the Soft-Actor Critic (SAC) algorithm to train an agent for the control of a single finger. SAC is an off-policy learning algorithm and is preferred for training robotic systems due to its sample efficiency, as it can learn from both past and current data. SAC is also preferred due to its ability to handle continuous action spaces, incorporate entropy regularisation for better exploration, utilise both policy and value functions, and exhibit robustness and stability during learning.

The single-fingered environment of the hand has 4 DOFs and 5 tendons. Learning curves for the average episodic return and episodic length are shown in Figure 14 and Figure 15. The maximum episodic length is 200 steps, and the maximum episodic return for the environment is 1,800 which corresponds to solving the task within the first step i.e., 80ms. The final model had an average episodic return of 1,100 and an average episodic length of 194 steps. After training, the model was evaluated to inspect the tendon tensions used by the model as described in Section 2.4. Distributions of the tension applied in each of the tendons are shown in Figures 16-20. The initial tension limit for all the tendons is 5N. The results show that the agent has optimized for tension magnitude by using less than 5N most of the time. Figure 18 shows that the tendon that requires the highest tension is the Extensor Digitorum Communis - a single tendon that extends the finger at 3 joints. Figure 18 also hints that the tension limit for this tendon will need to the increased as the agent gets to the tendon's tension limit very often.

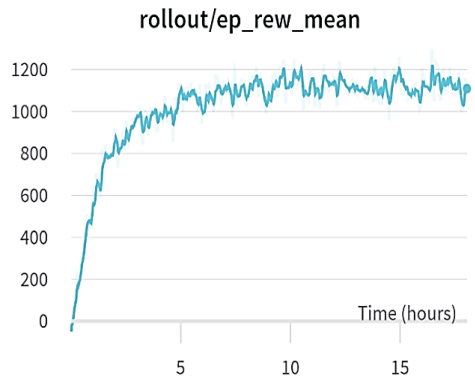

Figure 14. Average episodic return of SAC agent on single-finger environment

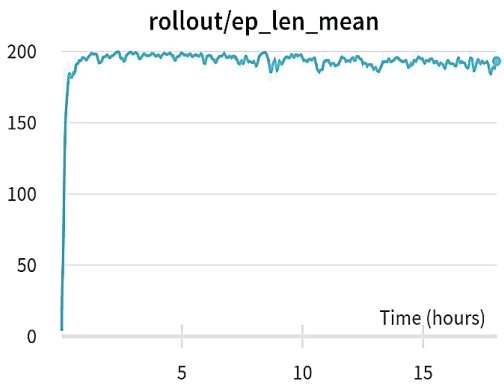

Figure 15. Average episodic length of SAC agent on single-finger environment

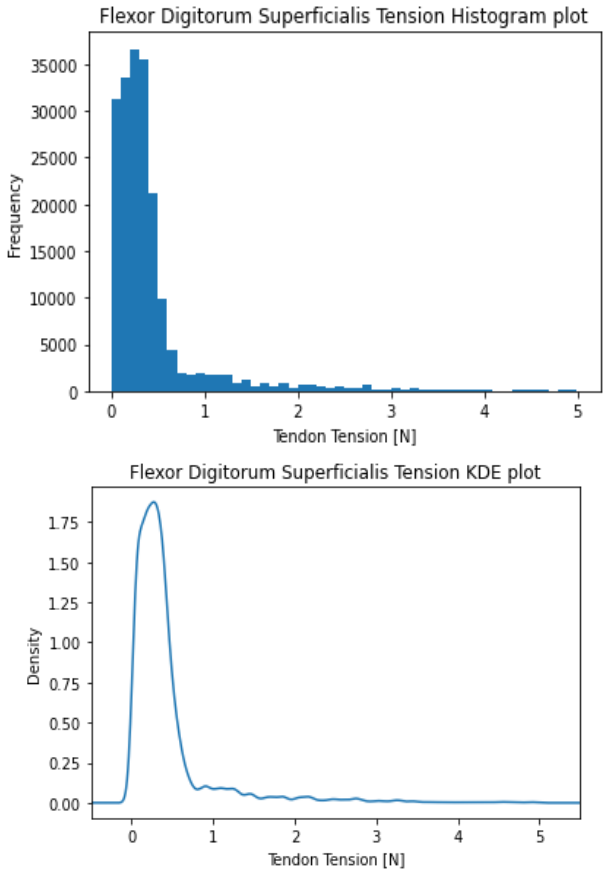

Figure 16. Tension distribution for the flexor digitorum superficialis

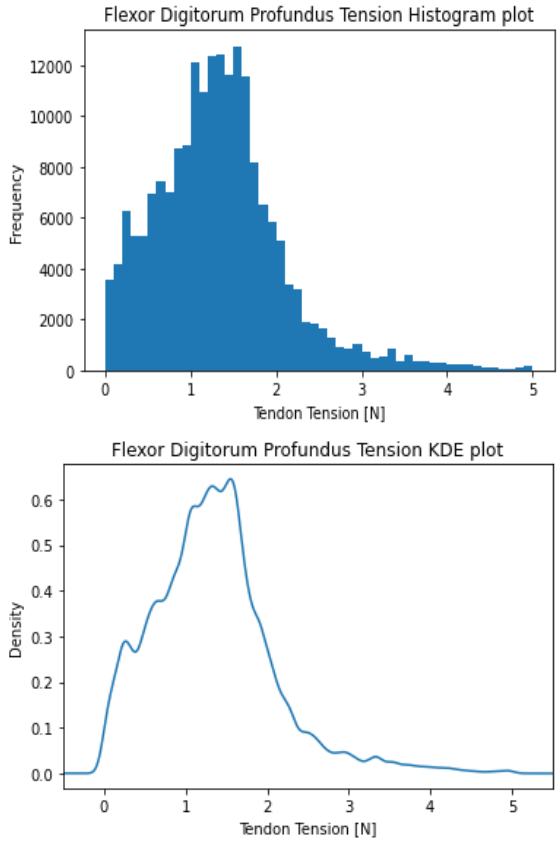

Figure 17. Tension distribution for the flexor digitorum profundus

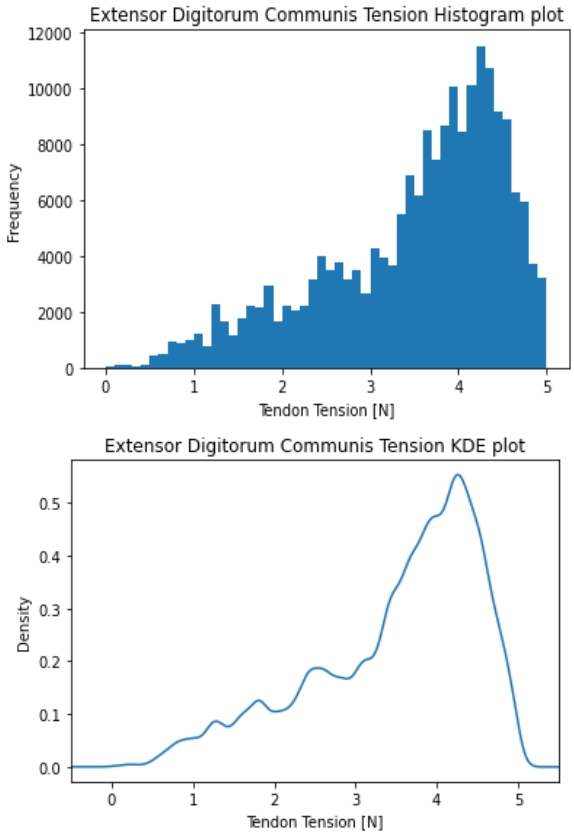

Figure 18. Tension distribution for the extensor digitorum communis

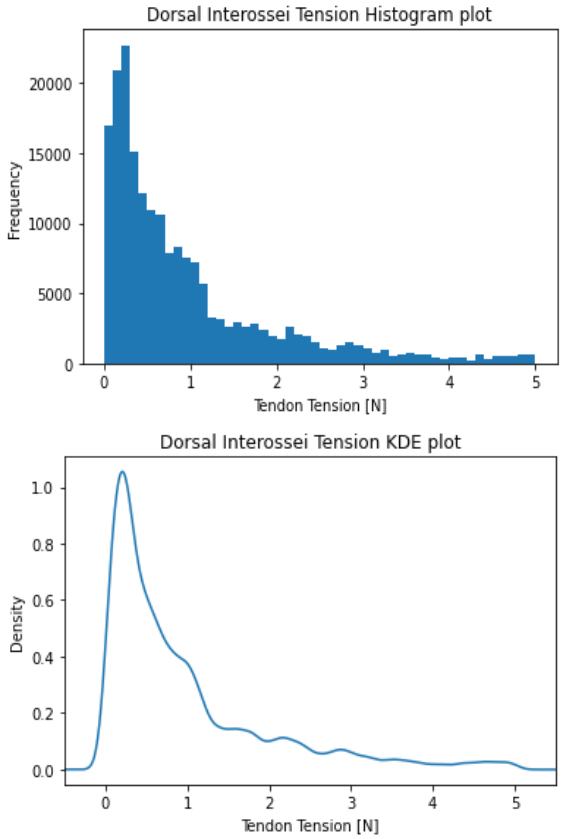

Figure 19. Tension distribution for the dorsal interossei

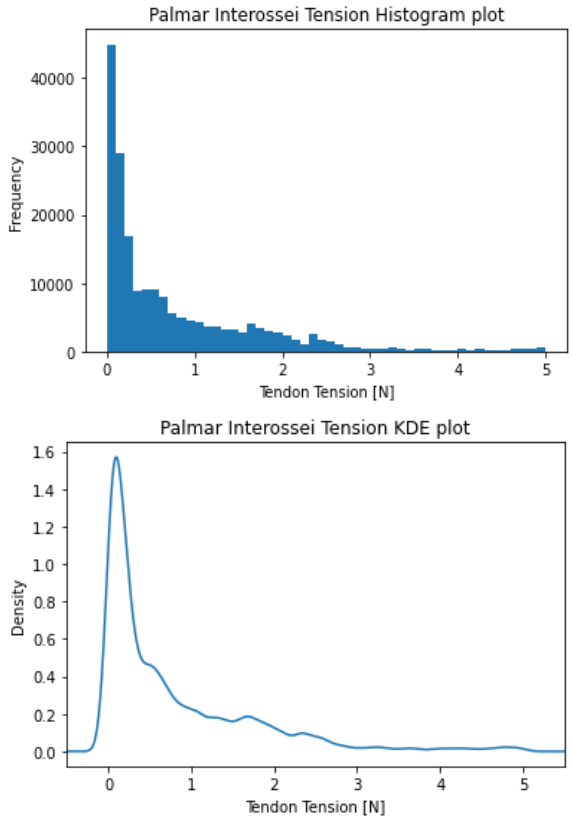

Figure 20. Tension distribution for the palmar interossei

3.5 Schematics of the UI Hand I

Figure 21 shows the system schematic of UI Hand I include (1) the Leap Motion Controller and (2) a host computer for teleoperation; (3) a Raspberry PI onboard the robotic hand for computing and communication; (4) a power supply; (5) the motor driver board that drive the motors; (6) dc motors; (7) and the link assembly of the robotic hand.

The Leap Motion controller was chosen for teleoperation as it is a cheaper motion capture device for the hand when compared to many motion caption gloves. Compared to other single-board computers like BeagleBone Black and Jetson Nano, the Raspberry Pi 4 SBC also provided a good balance between performance and cost. While the Raspberry Pi 4 doesn't provide a GPU like the Nvidia Jetson Nano, it has a speed good enough for running simple inference on the trained RL model. A dedicated power supply unit is chosen to provide enough current supply to the 34 motors of the hand during operation.

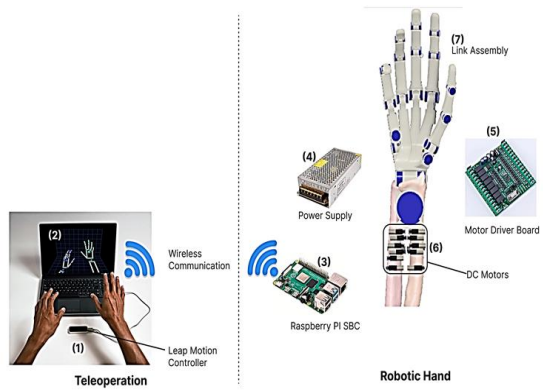

Figure 21. System schematic of the proposed UI Hand I

3.6 Cost estimation

Table 2 shows the cost analysis for the development of our robotic hand.

Table 2. Cost estimation for the proposed UI Hand I

Component	Unit Cost ($/unit)	Quantity	Total ($)
3D Printing of PLA Links	219.40/Kg	0.5Kg	109.70
Tendons (Spectra Fibre)	48.50/spool	1 spool	48.50
IND-GM-609-26.45	9.70/unit	10	97.00
IND-GM-609-136	10.62/unit	17	180.54
IND-GM-609-699	11.55/unit	4	46.20
Raspberry Pi (Pi 4 Model B)	230.95/unit	1	230.95
Leap Motion Controller	265.59/unit	1	265.59
Tactile Sensor	9.24/unit	20	184.80
Surgical Gloves	9.24/pack	1	9.24
Power Supply and motor controller board	69.28/unit	1	69.28
Total		**1, 241.80**	

3.7 Future work

As we continue with the development of the UI Hand I, the implementation of the RL model and the results obtained from simulation will be finetuned. Subsequently, the model of the mechanics of the hand will be implemented, and the actuation system will be verified. The trained model will be deployed on the real hand using the various Sim2Real techniques discussed in Section 2.7, and the performance of the control system will be evaluated on the real hand. In a future iteration of the UI Hand, we will include a tactile sensing subsystem, which will improve the performance of the robotic hand for in-hand grasping and manipulation tasks [44].

4. CONCLUSION

The study aims to improve the fidelity of biomimetic robotic hand design. We achieve this by using methods and models that help to mimic both the form and mechanical features of the human hand. This yields a highly dexterous, 26 degrees of freedom anthropomorphic robotic hand, which captures all the degrees of freedom in the human hand and wrist. We achieved robust control by using a Deep Reinforcement Learning agent that was trained using the Soft-Actor Critic algorithm for teleoperation. The successful implementation of the UI Hand I will open up enhanced dexterity and automation in applications such as spacewalks, industrial operations, construction, prosthetics, and many more.

ACKNOWLEDGMENT

The Authors extend their appreciation to the Founder and Management of Afe Babalola University; Ado Ekiti for the payment of Article Processing Charges (APC) of this manuscript.

REFERENCES

[1] Xu, Z., Kumar, V., Todorov, E. (2013). A low-cost and modular, 20-DOF anthropomorphic robotic hand: Design, actuation and modeling. In 2013 13th IEEE-RAS International Conference on Humanoid Robots (Humanoids), Atlanta, GA, USA, pp. 368-375. https://doi.org/10.1109/HUMANOIDS.2013.7030001

[2] Engel, J. (2004). Surgical anatomy of the hand Hans-martin Schmidt, Ulrich Lanz Thieme ISBN: 3 13 125261 8 Price € 159.00. Journal of Hand Surgery, 29(4): 410-410. https://doi.org/10.1016/J.JHSB.2004.04.001

[3] Cutkosky, M.R. (1989). On grasp choice, grasp models, and the design of hands for manufacturing tasks. IEEE Transactions on Robotics and Automation, 5(3): 269-279. https://doi.org/10.1109/70.34763

[4] Rajeswaran, A., Kumar, V., Gupta, A., Vezzani, G., Schulman, J., Todorov, E., Levine, S. (2017). Learning complex dexterous manipulation with deep reinforcement learning and demonstrations. arXiv preprint arXiv:1709.10087.

[5] Liow, L., Clark, A.B., Rojas, N. (2019). Olympic: A modular, tendon-driven prosthetic hand with novel finger and wrist coupling mechanisms. IEEE Robotics and Automation Letters, 5(2): 299-306. https://doi.org/10.1109/LRA.2019.2956636

[6] Mnyusiwalla, H., Vulliez, P., Gazeau, J.P., Zeghloul, S. (2015). A new dexterous hand based on bio-inspired finger design for inside-hand manipulation. IEEE Transactions on Systems, Man, and Cybernetics: Systems, 46(6): 809-817. https://doi.org/10.1109/TSMC.2015.2468678

[7] Tian, L., Magnenat Thalmann, N., Thalmann, D., Zheng, J. (2017). The making of a 3D-printed, cable-driven, single-model, lightweight humanoid robotic hand. Frontiers in Robotics and AI, 4: 65. https://doi.org/10.3389/frobt.2017.00065

[8] Mańkowski, T., Tomczyński, J., Walas, K., Belter, D. (2020). PUT-hand—Hybrid industrial and biomimetic gripper for elastic object manipulation. Electronics, 9(7): 1147. https://doi.org/10.3390/electronics9071147

[9] Vulliez, P., Gazeau, J.P., Laguillaumie, P., Mnyusiwalla, H., Seguin, P. (2018). Focus on the mechatronics design of a new dexterous robotic hand for inside hand manipulation. Robotica, 36(8): 1206-1224. https://doi.org/10.1017/S0263574718000346

[10] Wang, T., Geng, Z., Kang, B., Luo, X. (2019). Eagle Shoal: A new designed modular tactile sensing dexterous hand for domestic service robots. In 2019 International Conference on Robotics and Automation (ICRA), Montreal, QC, Canada, pp. 9087-9093. https://doi.org/10.1109/ICRA.2019.8793842

[11] Li, C., Gu, X., Xiao, X., Zhu, G., Prituja, A.V., Ren, H. (2019). Transcend anthropomorphic robotic grasping with modular antagonistic mechanisms and adhesive soft modulations. IEEE Robotics and Automation Letters, 4(3): 2463-2470. https://doi.org/10.1109/LRA.2019.2906556

[12] He, Z., Yurievich, R.R., Shimizu, S., Fukuda, M., Kang, Y., Shin, D. (2020). A design of anthropomorphic hand based on human finger anatomy. In 2020 International Symposium on Community-centric Systems (CcS), Tokyo, Japan, pp. 1-5.

https://doi.org/10.1109/CcS49175.2020.9231423
[13] Xu, Z., Kolev, S., Todorov, E. (2014). Design, optimization, calibration, and a case study of a 3D-printed, low-cost fingertip sensor for robotic manipulation. In 2014 IEEE International Conference on Robotics and Automation (ICRA), Hong Kong, China, pp. 2749-2756. https://doi.org/10.1109/ICRA.2014.6907253
[14] Tian, L., Magnenat-Thalmann, N., Thalmann, D., Zheng, J. (2018). A methodology to model and simulate customized realistic anthropomorphic robotic hands. In Proceedings of Computer Graphics International 2018, New York, USA, pp. 153-162. https://doi.org/10.1145/3208159.3208182
[15] Gama Melo, E.N., Aviles Sanchez, O.F., Amaya Hurtado, D. (2014). Anthropomorphic robotic hands: A review. Ingeniería y Desarrollo, 32(2): 279-313. http://www.scielo.org.co/scielo.php?script=sci_abstract&pid=S0122-34612014000200007.
[16] Xu, Z., Todorov, E. (2016). Design of a highly biomimetic anthropomorphic robotic hand towards artificial limb regeneration. In 2016 IEEE International Conference on Robotics and Automation (ICRA), Stockholm, pp. 3485-3492. https://doi.org/10.1109/ICRA.2016.7487528
[17] Tang, A., Varacallo, M. (2021). Anatomy, shoulder and upper limb, hand carpal bones. In StatPearls [Internet]. StatPearls Publishing.
[18] Albrecht, I., Haber, J., Seidel, H.P. (2003). Construction and animation of anatomically based human hand models. In Proceedings of the 2003 ACM SIGGRAPH/Eurographics symposium on Computer animation, Saarbrücken, Germany, pp. 98-109.
[19] Panchal-Kildare, S., Malone, K. (2013). Skeletal anatomy of the hand. Hand Clinics, 29(4): 459-471. https://doi.org/10.1016/j.hcl.2013.08.001
[20] Aitken, S., Court-Brown, C.M. (2008). The epidemiology of sports-related fractures of the hand. Injury, 39(12): 1377-1383. https://doi.org/10.1016/j.injury.2008.04.012
[21] del Piñal, F., Moraleda, E., Rúas, J.S., de Piero, G.H., Cerezal, L. (2015). Minimally invasive fixation of fractures of the phalanges and metacarpals with intramedullary cannulated headless compression screws. The Journal of Hand Surgery, 40(4): 692-700. https://doi.org/10.1016/j.jhsa.2014.11.023
[22] Controzzi, M., Cipriani, C., Jehenne, B., Donati, M., Carrozza, M.C. (2010). Bio-inspired mechanical design of a tendon-driven dexterous prosthetic hand. In 2010 Annual International Conference of the IEEE Engineering in Medicine and Biology, Buenos Aires, Argentina, pp. 499-502. https://doi.org/10.1109/IEMBS.2010.5627148
[23] Kozin, S.H., Thoder, J.J., Lieberman, G. (2000). Operative treatment of metacarpal and phalangeal shaft fractures. JAAOS-Journal of the American Academy of Orthopaedic Surgeons, 8(2), 111-121.
[24] Ken Hub. (2022) Learn Anatomy. https://www.kenhub.com.
[25] Lee, S., Park, M., Lee, K., Lee, J. (2019). Scalable muscle-actuated human simulation and control. ACM Transactions on Graphics (TOG), 38(4): 1-13. https://doi.org/10.1145/3306346.3322972
[26] Ackerman, M.J. (1998). The visible human project. Proceedings of the IEEE, 86(3): 504-511. https://doi.org/10.1109/5.662875
[27] Nazma, E., Mohd, S. (2012). Tendon driven robotic hands: A review. International Journal of Mechanical Engineering and Robotics Research, 1(3): 350-357.
[28] Wilkinson, D.D., Weghe, M.V., Matsuoka, Y. (2003). An extensor mechanism for an anatomical robotic hand. In 2003 IEEE International Conference on Robotics and Automation, Taipei, Taiwan, pp. 238-243. https://doi.org/10.1109/ROBOT.2003.1241602
[29] Kaneko, M., Wada, M., Maekawa, H., Tanie, K. (1991). A new consideration on tendon-tension control system of robot hands. In Proceedings of 1991 IEEE International Conference on Robotics and Automation, Sacramento, CA, USA, pp. 1028-1029. https://doi.org/10.1109/ROBOT.1991.131727
[30] Palli, G., Borghesan, G., Melchiorri, C. (2012). Modelling, identification, and control of tendon-based actuation systems. IEEE Transactions on Robotics, 28: 277-290. https://doi.org/10.1109/TRO.2011.2171610
[31] Palli, G., Melchiorri, C., Vassura, G., et al. (2014). The DEXMART hand: Mechatronic design and experimental evaluation of synergy-based control for human-like grasping. The International Journal of Robotics Research, 33(5): 799-824. https://doi.org/10.1177/0278364913519897
[32] Zeng, C., Li, S., Jiang, Y., Li, Q., Chen, Z., Yang, C., Zhang, J. (2021). Learning compliant grasping and manipulation by teleoperation with adaptive force control. In 2021 IEEE/RSJ International Conference on Intelligent Robots and Systems (IROS), Prague, Czech Republic, pp. 717-724. https://doi.org/10.1109/IROS51168.2021.9636832
[33] Smith, N.C., Wilson, A.M., Jespers, K.J., Payne, R.C. (2006). Muscle architecture and functional anatomy of the pelvic limb of the ostrich (Struthio camelus). Journal of Anatomy, 209(6): 765-779. https://doi.org/10.1111/j.1469-7580.2006.00658.x
[34] Li, Z.M., Zatsiorsky, V.M., Latash, M.L. (2000). Contribution of the extrinsic and intrinsic hand muscles to the moments in finger joints. Clinical biomechanics, 15(3): 203-211. https://doi.org/10.1016/S0268-0033(99)00058-3
[35] Li, Z.M., Zatsiorsky, V.M., Latash, M.L. (2001). The effect of finger extensor mechanism on the flexor force during isometric tasks. Journal of Biomechanics, 34(8): 1097-1102. https://doi.org/10.1016/S0021-9290(01)00061-6
[36] Xu, H., Luo, Y., Wang, S., Darrell, T., Calandra, R. (2022). Towards learning to play piano with dexterous hands and touch. In 2022 IEEE/RSJ International Conference on Intelligent Robots and Systems (IROS), Kyoto, Japan, pp. 10410-10416. https://doi.org/10.1109/IROS47612.2022.9981221
[37] Haarnoja, T., Zhou, A., Hartikainen, K., Tucker, G., Ha, S., Tan, J., Kumar, V., Zhu, H., Gupta, A., Abbeel, P., Levine, S. (2018). Soft actor-critic algorithms and applications. arXiv preprint arXiv:1812.05905. https://doi.org/10.48550/arXiv.1812.05905
[38] Yu, C., Wang, P. (2022). Dexterous manipulation for multi-fingered robotic hands with reinforcement learning: A review. Frontiers in Neurorobotics, 16: 861825. https://doi.org/10.3389/fnbot.2022.861825
[39] Andrychowicz, O. M., Baker, B., Chociej, M.,

Jozefowicz, R., McGrew, B., Pachocki, J., and Zaremba, W. (2020). Learning dexterous in-hand manipulation. The International Journal of Robotics Research, 39(1), 3-20. https://doi.org/10.1177/0278364919887447

[40] Caggiano, V., Wang, H., Durandau, G., Sartori, M., Kumar, V. (2022). MyoSuite--A contact-rich simulation suite for musculoskeletal motor control. arXiv preprint arXiv:2205.13600. https://doi.org/10.48550/arXiv.2205.13600

[41] Akkaya, I., Andrychowicz, M., Chociej, M., Litwin, M., McGrew, B., Petron, A., Paino, A., Plappert, M., Powell, G., Ribas, R., Schneider, J., Tezak, N.A., Tworek, J., Welinder, P., Weng, L., Yuan, Q., Zaremba, W., Zhang, L.M. (2019). Solving Rubik's cube with a robot hand. ArXiv, abs/1910.07113. https://doi.org/10.48550/arXiv.1910.07113

[42] Ultraleap. (2022) https://www.ultraleap.com/leap-motion-controller-overview/.

[43] Ackerman, M.J. (2022). The visible human project. Information Services & Use, 42(1): 129-136. https://doi.org/10.3233/ISU-210145

[44] Yousef, H., Boukallel, M., Althoefer, K. (2011). Tactile sensing for dexterous in-hand manipulation in robotics—A review. Sensors and Actuators A: Physical, 167(2): 171-187. https://doi.org/10.1016/J.SNA.2011.02.038